

Document downloaded from:

<http://hdl.handle.net/10251/49602>

This paper must be cited as:

Guenbour, A.; Escrivá Cerdán, C.; Blasco Tamarit, ME.; García García, DM.; García Antón, J.; Guenbour, A. (2012). Effect of potential formation on the electrochemical behaviour of a highly-alloyed austenitic stainless steel in contaminated phosphoric acid at different temperatures. *Electrochimica Acta*. 80:248-256. doi:10.1016/j.electacta.2012.07.012.



The final publication is available at

<http://dx.doi.org/10.1016/j.electacta.2012.07.012>

Copyright Elsevier

**EFFECT OF POTENTIAL FORMATION ON THE ELECTROCHEMICAL
BEHAVIOUR OF A HIGHLY-ALLOYED AUSTENITIC STAINLESS STEEL
IN CONTAMINATED PHOSPHORIC ACID AT DIFFERENT
TEMPERATURES**

**Escrivà-Cerdán^a, C., Blasco-Tamarit^a, E., García-García^a, D.M., García-Antón,
J.^{a,*}, Guenbour, A^b**

*^aIngeniería Electroquímica y Corrosión (IEC). Universitat Politècnica de Valencia.
c/Camino de Vera, s/n 46022 Valencia, Spain.*

**Tel. 34-96-387 76 39, Fax. 34-96-387 76 39, e-mail. jgarciaa@iqn.upv.es*

*^bLaboratoire de Corrosion-Electrochimie, Faculté des Sciences, Université Mohammed
V-Agdal, BP 1014 Rabat, Morocco.*

ABSTRACT

The electrochemical behaviour of the highly-alloyed austenitic stainless steel UNS N08031 (Alloy 31) in a contaminated phosphoric acid solution is studied using potentiodynamic curves, EIS and Mott-Shottky. The relative stability of the films formed on Alloy 31 has been studied after a pre-passivated treatment at 0.3, 0.5, 0.8 and 1 V_{Ag/AgCl} potentials within the passive domain. The protection of Alloy 31 was provided by the inner oxide film, while the outer film was more defective. The electronic-semiconducting properties of the passive films have been correlated to corrosion resistance. Passivated Alloy 31 at 0.8 V_{Ag/AgCl} showed lower concentration of charge carriers, which beneficially affects the protecting and electronic properties of the passive oxide film.

Keywords: Stainless steel, Acid solution, Passivity, EIS, Mott-Schotky

1. INTRODUCTION

The protective capability of the passive film formed on stainless steel is related to the composition of the alloy and the aggressiveness of the environment to which it is exposed. The corrosion resistance of all types of austenitic stainless steel is based on the bilayer structure of the formed passive films spontaneously on their surface in aqueous solutions. These films act as a barrier layer, separating the metal's surface from the corrosive ions in the environment. Thus the understanding of the corrosion resistance of stainless steel lies in comprehending the properties of the passive films formed on the steel.

Based on a surface analysis, Olefjord and Elfström [1] proposed a model for passive films formed on austenitic stainless steels in acidic solutions. They observed that the outer part consists mainly of an hydroxide film on top of an oxide layer. This oxy-hydroxide film grows on a nickel-enriched layer, the origin of which is the selective oxidation of Fe and Cr during anodic polarisation [2]. Recent investigations confirm the fact that the passive film can be described as having a bilayer structure [3-5]. In this sense, it has been widely accepted [6-10] that the outer layer is rich in Fe^{3+} species and the inner layer consists of an anhydrous mixed Fe-Cr-Ni oxide [3]. However, in phosphoric acid media (H_3PO_4), the composition of the outer layer seems to change; according to other studies [11-13], iron-phosphate species can precipitate at the interface and be incorporated to the passive layer, forming an outer porous film.

The passivation behaviour and corrosion resistance of stainless steels in this medium have been mainly studied by potentiodynamic polarisation [14-18], although other

techniques have also been used, namely electrochemical impedance spectroscopy (EIS), to shed more light on the mechanisms of electropolishing in phosphoric acid [19-22]. More recently, this technique has been used to evaluate the corrosion behaviour of surgical grade austenitic stainless steel (316L SS) treated with various H_3PO_4 concentrations [23].

As a consequence of the semiconducting nature, the electronic properties of passive films strongly affect corrosion resistance, as proposed elsewhere [24-27]. Depending on the predominant defects present in the passive oxide layer, either p-type or n-type behaviours are observed. Passive oxide films with a metallic ion deficiency or cation-vacancy excess generally behave as p-type. Whereas passive films with cation excess in interstitial sites or anion vacancies behave as n-type. Mott-Schottky analysis has shown to be an important in-situ method for investigating the semiconducting properties of passive films [9, 28-30].

It has often been assumed that the semiconducting behaviour of austenitic stainless steels and Fe-Cr alloys reflects the duplex structure of the passive films. The majority of authors [6-10] consider that the inner barrier layer is consisting mainly of chromium(III) oxide, which behaves as a p-type semiconductor, whereas the outer region of the passive film is composed mainly of iron(III) oxide, which behaves as an n-type semiconductor [4, 27]. The Mott-Schottky analysis showed that the barrier layers on the stainless steels were n-type, probably due to the inhibition of cation-vacancy generation relative to oxygen-vacancy generation and metallic interstitials generation [31]. During the last years, the electrochemical behaviour of passive films formed on austenitic stainless steels has been widely studied [4, 28, 32-36]. Ferreira et al. [34] and Fattah-

alhosseini [33] reported the influence of temperature on film formation, and other researchers [9, 28, 32] have shown the influence of the potential formation of passive films in acid solutions. Other studies have analysed the role of nitrogen [28] in acidic solutions or the influence of added alloying components (e.g. Ni and Mo) [37-39] on the anodic passive films of stainless steels and Cr-Fe alloys.

The aim of the present work is to evaluate the electrochemical and semiconducting behaviour of the highly alloyed austenitic stainless steel UNS N08031 (Alloy 31) in a 40 wt.% phosphoric acid solution contaminated with 2 wt.% H₂SO₄ and 0.06 wt.% KCl. The concentration of these impurities in the solution has been chosen according to the industrial conditions [14, 16, 40, 41]. However, it is important to point out that fluorides are likely to be present in an industrial solution.

2. EXPERIMENTAL

2.1. Material and test solution

The material tested was the highly-alloyed austenitic stainless steel UNS N08031 (Alloy 31) provided by Thyssen Krupp VDM. The material composition is shown in **Table 1**. Alloy 31 electrodes were cylindrically shaped (8 mm in diameter and 55 mm long) and covered with a polytetrafluoroethylene (PTFE) coating. The area exposed to the solution was 0.5 cm².

The cross-section of the electrodes was ground down with wet emery paper of decreasing grit size (500 - 4000). After polishing, the samples were rinsed with distilled water and dried with a stream of air just before the immersion.

Material was tested in a 40 wt.% phosphoric acid (5.5 M) solution contaminated with 2 wt% H₂SO₄ (0.25 M) and 0.06 wt.% KCl, typical concentrations in the phosphoric acid industry [41]. The solution was prepared with distilled water and the pH of the solution was 0.42.

2.2. Experimental methods

A conventional three-electrode cell, held at a constant temperature, was used for the electrochemical analysis of Alloy 31. A platinum counter-electrode and a silver/silver chloride (Ag/AgCl) 3 M potassium chloride reference electrode were used in the cell. All the electrode potentials were referred to the Ag/AgCl scale. The experiments were conducted under thermostated conditions at 20, 40, 60 and 80 °C in order to study the influence of temperature on the electrochemical behaviour and semiconducting properties of Alloy 31.

The electrochemical tests were conducted in deaerated solution by bubbling N₂ into the solution for 20 min before the test, and then the nitrogen atmosphere was maintained over the liquid surface during the whole test.

Anodic polarisation curves were measured potentiodynamically with a Solartron 1287 potentiostat at a scan rate of 0.1667 mV/s from $-0.4 V_{\text{Ag/AgCl}}$ to the anodic direction,

according to ASTM G5 [42]. The polarisation curves were used to determine the passive potential ranges of Alloy 31 in the solution studied. Before each polarisation measurement, the working electrodes were initially polarised in four steps from the OCP values (approximately $0.2 V_{\text{Ag/AgCl}}$) to 0, -0.2 and $-0.4 V_{\text{Ag/AgCl}}$. The potential of $-0.4 V_{\text{Ag/AgCl}}$ was maintained for 1 hour in order to remove the air-formed oxide on the surface [9, 35, 43] and to create reproducible initial conditions. It has been found that during this pre-treatment, the air-formed oxide on the surface is removed [35]. Moreover, at this potential Hydrogen has no obvious effect on the semiconducting properties of the subsequent passive film.

Besides the polarisation curves, potentiostatic current-time transients were recorded. The samples were reduced potentiostatically at $-0.4 V_{\text{Ag/AgCl}}$ for 1 hour and the working electrode was anodically polarised to the selected film formation potentials of 0.3, 0.5, 0.8 and $1 V_{\text{Ag/AgCl}}$, which were in the passive region of the potentiodynamic polarisation curves. A stationary stage of layer growth was considered, applying each potential for 1 hour before the impedance and capacitance measurements.

Once the passive film was formed, the electrochemical impedance spectroscopy (EIS) measurements were taken in the range between 10^5 and 10^{-3} Hz with voltage amplitude ± 5 mV. Capacitance measurements were also taken on the anodic films formed at 0.3, 0.5, 0.8 and $1 V_{\text{Ag/AgCl}}$, at a frequency of 3 kHz using a 10 mV rms ac signal and a step rate of 25 mV, in the cathodic direction. All EIS and capacitance measurements were recorded from the potential at which the passive film was formed, using an Autolab PGSTAT302N potentiostat.

3. RESULTS AND DISCUSSION

3.1. Potentiodynamic polarisation behaviour

Figure 1 shows the potentiodynamic polarisation plots of Alloy 31 in the contaminated phosphoric acid solution at different temperatures. Alloy 31 displays similar polarisation curves at all temperatures, showing a very wide potential domain of passivity, generally in the potential range between 0.3 and 1 V_{Ag/AgCl}. Thus, this has been the selected potential range to study the properties of the passive film formed on Alloy 31. From the 1 V_{Ag/AgCl} potential, the sharp increase in current density indicates the breakdown of the passive film, showing the transpassive region of Alloy 31 in the phosphoric acid solution.

Temperature also affects the cathodic branch, increasing the cathodic current densities, i.e. temperature favours the cathodic reaction [44, 45] as well as the Hydrogen Evolution Reaction (HER), which results in a greater generation of H₂ due to a decrease in the overpotential needed for this reaction when temperature increases [46]. The kinetics of the oxidation reactions is also favoured with temperature [44, 47-50], as can be observed on the anodic branch of the polarisation curves, although the higher current density values registered within the passive region are attributed to the growth of oxide films on metallic surface [2, 51, 52]. In general, Alloy 31 registered a stable current density in the passive domain, although at the highest temperatures (60 and 80 °C) these values slightly and progressively increase. Therefore, the results of the polarisation curves reveal that higher temperatures favour the thickening of the passive films.

The displacement of the corrosion potentials with temperature is in agreement with the results reported by other authors [44, 52, 53], who studied the effects of the solution temperature on different stainless steels and seems to be also related to the increase in cathodic current densities [44]. Recently, a complete study on the effect of temperature on the electrochemical parameters of Alloy 31 in contaminated phosphoric acid has been published [46].

3.2. Electrochemical impedance analysis

To investigate the relative stability of the passive films formed on Alloy 31, EIS measurements were recorded at applied potentials after passive film generation. Based on the shape of the polarisation curves, the different potentials chosen (0.3, 0.5, 0.8 and 1 V_{Ag/AgCl}) lie within the passive region.

For the EIS results to be valid, the electrochemical system should comply with three requirements formulated for the constraints of the linear system theory (LST) i.e. causality, linearity and stability [54-56]; otherwise the EIS results will be invalid [54-56]. Thus, the way to validate the EIS results is the Kramers-Kronig (K-K) transformation [55]. The K-K transforms have been applied to the EIS measurements by transforming the real axis into the imaginary axis and the imaginary axis into the real axis. **Figure 2** shows the similar results between the experimental points and the corresponding K-K transforms, confirming the compliance of the system with the linear systems theory.

The impedance responses are presented in Nyquist and Bode formats in **Figure 3** for the different temperatures studied (20, 40, 60 and 80 °C). All impedance spectra present a somewhat unfinished capacitive arc which is temperature dependent, as evidenced by the overall decrease of impedance values with temperature. Bode plots in **Figure 3** depict two time constants, at high- and low-frequencies. This feature is often considered as the response of an inhomogeneous film composed of a compact inner layer and a less compact (porous) outer layer [57-60]. According to this behaviour, a hierarchically distributed equivalent circuit, reproduced in **Figure 4**, has been previously reported [9, 28, 57-63].

The modulus of the phase angle maxima is lower than 90° in all EIS spectra (**Figure 3**); such behaviour can be interpreted as a deviation from ideal capacitor behaviour. Therefore, the use of a constant phase element (CPE) was necessary to account for the non-ideal behaviour of the capacitive elements, due to the distribution of relaxation times as a consequence of heterogeneities on the electrode surface [64]. The impedance of this element is defined as [54]:

$$Z_{CPE} = \frac{1}{Q \cdot (j\omega)^\alpha} \quad (1)$$

where Q is the CPE constant, ω is the angular frequency (rad/s), $j^2=-1$ is the imaginary number and α is the CPE exponent. Depending on α , CPE can represent resistance ($\alpha=0$, $Z_0=R$), capacitance ($\alpha=1$, $Z_0=C$), or Warburg impedance ($\alpha=0.5$, $Z_0=W$).

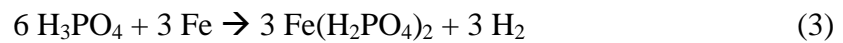
The CPE elements, Q , have been converted into a pure capacitance (C) by means of the following equation [64]:

$$C = \frac{(Q \cdot R)^{1/\alpha}}{R} \quad (2)$$

The circuit represented in **Figure 4** has been used to explain the passivity behaviour of Alloy 31 in the contaminated phosphoric acid solution at 20, 40, 60 and 80 °C. The quality of data fitting to the equivalent circuit proposed was evaluated with the chi-squared (χ^2) values, which were lower than 10^{-3} , and the error percentages of the individual components of the equivalent circuit fitted. This is also shown in **Figure 3**, where the simulated data are shown as solid lines. Other equivalent circuits were tested, with a series association of two R-CPE elements [65, 66] and with other functions [67, 68], namely Young impedance instead of a CPE, but the fitting errors were high. Thus, the physical description of the model adopted in this work is that R_1 , C_1 and R_2 , C_2 correspond to the resistance and capacitance of the outer porous layer and inner oxide layer, respectively. In this sense, the high frequency time constant is represented by the resistance of the solution in the defects of the porous film (R_1) and the double layer capacitance in the defects (C_1). The second time constant at low frequencies is assigned to the areas covered with the passive oxide film (protective oxide) and it is represented by the R_2/C_2 parallel combination. Both parameters, R_2 and C_2 , represent the electrical resistance and the capacitance of the passive oxide film formed as an inner layer on Alloy 31. The resistance at very high frequencies corresponds to the uncompensated resistance of the solution (R_s), which remains almost constant in all tests. In fact, at high frequencies ($10^4 - 10^5$ Hz), the absolute impedance curve is almost independent of

frequency with a phase angle of 0° , representing that the R_s is almost constant ($R_s \cong 1.2 \Omega \text{ cm}^2$).

The compact inner layer, known as barrier layer, is composed principally of chromium oxides and is the major contributor. The outer porous film in phosphoric acid media is composed of iron phosphates [13]. Phosphate species can precipitate with dissolved iron species to form iron phosphates since these compounds are characterised by a low solubility. Therefore, precipitation of iron phosphate ($\text{Fe}_3(\text{PO}_4)_2$) occurs at the interface, according to the following reactions [11]:



In stainless steels, as a result of the low oxidative capacity of the surface, a predominant formation of soluble phosphate $\text{Fe}(\text{H}_2\text{PO}_4)_2$ occurs, which is responsible for porous film formation [12], as shown schematically in **Figure 4**.

The resistance, capacitance and α values of the outer and inner layers obtained by adjusting the experimental data show in **Figure 3** are summarised in **Table 2** as a function of the temperatures at different applied potentials. In all cases, the CPE_1 exponents, α_1 , have values close to 0.9, which indicates that the interpretation of the CPE_1 element as a capacitance should be acceptable, whereas the values of α_2 were between 0.6 and 0.8. According to the electrical parameters obtained, the resistance of the inner oxide layer (R_2) is significantly larger than the values associated with the outer porous layer (R_1), which is consistent with the chosen physical model. These results

indicate that the protection provided by the passive film was predominantly due to the barrier layer. Similar results were obtained by other authors [58, 69]. The resistance of the outer porous layer R_I depends strongly on the existence of pores or defects, into which the electrolyte can penetrate and thus, R_I provides a sensitive indication of the appearance of defects in the passive film. As a result, if the outer porous layer is very porous, the parameter R_I may correspond approximately to the resistance of the electrolyte inside the pores [58]. In the present study, the values of R_I are higher than those of R_s for all the conditions studied, although the outer layer exhibits a resistance of the order of $10^2 \Omega \text{ cm}^2$ and therefore, it can be considered as a thin and defective or porous film, as reported by other authors [58].

It can be seen in **Table 2** that R_I slightly decreases as temperature increases, which suggests that temperature favours the formation of a more porous film. This behaviour is probably related to the fact that at lower temperatures the outer porous layer is more stable as a result of the predominance of more stable phosphate iron compounds, resulting in higher resistances. Also the values of R_I are observed to decrease as the formation potential is increased from 0.3 to 0.8 $V_{\text{Ag/AgCl}}$, while at the formation potential of 1 $V_{\text{Ag/AgCl}}$, R_I has the highest values, indicating that the outer film is less defective. This behaviour might be due to the proximity to the transpassive region, which could lead to a distortion of the outer porous layer due to the partially blocked pores [70].

C_I values are in the order of those expected to the double layer capacitance [54] and hardly change with temperature at applied potentials of 0.3, 0.5 and 0.8 $V_{\text{Ag/AgCl}}$, with a slight decrease in C_I values at higher potentials.

The capacitance data obtained from EIS can be correlated with the thickness of the passive film layer [54, 71] using Eq. (5), which is valid for the parallel plate capacitor model:

$$C = \frac{(\varepsilon \cdot \varepsilon_0)}{d} \quad (5)$$

where ε denotes the relative dielectric constant of the layer, ε_0 is vacuum permittivity ($8.85 \cdot 10^{-14} \text{ F cm}^{-1}$) and d is the layer thickness. However, it is difficult to obtain an accurate thickness value of the passive film when the dielectric constant is not well established, although a value of 15.6 has been reported in the literature for austenitic stainless steels [10, 27]. Moreover, due to the open porous structure, it is difficult to calculate the thickness of the outer layer from the C_1 values [72]. Nevertheless, since capacitance is inversely proportional to layer thickness, the capacitive response of the alloys can give an indication of how the thickness of the passive film changes when changing the applied potentials.

The C_1 values suggest the thickening of the outer layer when the applied potential increases. In spite of film thickening, the evolution observed in R_1 suggests that the film becomes more defective as potential increases in the range of 0.3 - 0.8 $V_{\text{Ag}/\text{AgCl}}$. In fact, some authors have correlated this trend with the formation of a more porous film (higher effective area) [58].

On the other hand, the parameters associated with the inner oxide film, R_2 and C_2 , are more sharply affected by temperature and formation potential. R_2 clearly decreases when temperature increases, which suggests that the films' electrical conductivity

increases, as expected in a semiconductor. This is in contrast to the trend with the applied potential, which is observed to increase, except for the applied potential of 1 $V_{Ag/AgCl}$. The capacitance of the barrier layer, C_2 , hardly changes with the applied potential from 0.3 to 0.8 $V_{Ag/AgCl}$, taking values in the range of $10^2 - 10^3 \mu F \cdot cm^{-2}$. However, the barrier layer capacitance (C_2) increases considerably at 1 $V_{Ag/AgCl}$. According to expression (5), the relatively high capacitance values may indicate that the inner oxide film becomes thinner and this is specially observed at the potential near the transpassive region (1 $V_{Ag/AgCl}$).

The parameters obtained for the inner layer indicate that this layer is thin and compact [58, 69], which is indicated by the high capacitance and resistance values, of the order of $10^5 \Omega cm^2$. This is clearly observed after passive film formation at 0.8 $V_{Ag/AgCl}$, since the resistance of the oxide film is higher at 20 °C. However, R_2 exhibited high values even at 1 $V_{Ag/AgCl}$, indicating that the passive film formed on Alloy 31 still provides significant protection.

3.3. Mott-Schottky analysis

The Mott-Schottky (M-S) analysis has been employed to determine the electronic properties of the passive films formed on Alloy 31 in the 40 wt.% H_3PO_4 contaminated solution. In the M-S experiments, the specimens were passivated for 1 h at different formation potentials and the imaginary part of the impedance (Z''), measured at a frequency of 3 kHz, was recorded as a function of the potential, as the potential was swept in the negative direction at a sweep rate of 25 mV/s. The high sweep rate was used to avoid the electroreduction of the oxide layer and the change in the film

thickness during the measurements [28]. From the measured values of Z'' and the previously determined CPE α exponents, it was possible to calculate the CPE parameter, Q , and then the electrode capacitance by using Expression (2).

Capacitance results are usually frequency-dependent and thus, it is necessary to determine the frequency dependence of Alloy 31 in this medium. **Figure 5** shows Mott-Schottky measurements performed at different frequencies, i.e. from 1 to 5 kHz. The parameters obtained from such plots were found to be almost independent of frequency when this was higher than 2 kHz. Therefore, according to these previous measurements and other authors' results [9, 73] in this work a frequency of 3 kHz was applied for Mott-Schottky measurements.

Based on Mott-Schottky theory [25], the semiconducting characteristics of passive films can be explored by measuring the capacitance of the interface layer developed in the passive film and the Helmholtz layer, as a function of the applied electrode potential.

The measured capacitance can be described by this theory as: $\frac{1}{C} = \frac{1}{C_{SC}} + \frac{1}{C_H}$ where C_{SH} and C_H represent the space charge and the Helmholtz capacitance, respectively. However, since the capacitance of the space charge layer is very small compared with that of the Helmholtz layer, the measured interfacial capacitance can be regarded as that of the space charge layer when the potentials are applied with a sufficiently high frequency [9]. According to this theory, the space charge capacitance of p- and n-type semiconductors is given by Eq. (6) and (7), respectively:

$$\frac{1}{C^2} = \frac{-2}{\varepsilon \varepsilon_0 q N_A} \left(E - E_{FB} - \frac{kT}{q} \right) \quad (6)$$

$$\frac{1}{C^2} = \frac{2}{\varepsilon \varepsilon_0 q N_D} \left(E - E_{FB} - \frac{kT}{q} \right) \quad (7)$$

where N_A and N_D are the acceptor and donor density in the passive film, respectively, E is the applied potential, E_{FB} is the flat band potential, k is the Boltzman constant ($1.38 \cdot 10^{-23}$ J/K), T is the absolute temperature and q is the electron charge ($1.6 \cdot 10^{-19}$ C), while the meaning of ε_0 and ε has been already defined in equation (5).

Therefore, the validity of the M-S analysis is based on the assumption that the capacitance of the space-charge layer is much lower than that of the Helmholtz layer [8] and the data points on the $1/C_{SC}^2$ versus E plot can describe the semiconducting behaviour of the depletion region. N_A and N_D can be determined from the slope of this experimental data.

Figure 6 presents M-S plots for the passive films formed on Alloy 31 in the contaminated phosphoric acid solution at 20, 40, 60 and 80 °C and different film formation potentials. Firstly, it should be noted that at all film formation potentials, capacitances clearly increase with temperature. This trend is consistent with the results of the polarisation curves and EIS measurements. The diagrams obtained for film formation at 0.3, 0.5 and 0.8 V_{Ag/AgCl} (**Figure 6a, b and c**) show two regions in which a linear relationship between C^{-2} and E can be observed. In region I, the slope of the Mott-Schottky diagrams is close to zero, whereas region II in all plots reveals positive slopes, indicating the n-type semiconducting behaviour of the passive films.

Alloy 31 has high chromium content and as other studies have reported [31, 74, 75], an inner Cr enriched oxide film should be formed, which behaves as a p-type semiconductor. Moreover, its high Mo content and the strong acidic conditions of the solution ($\text{pH} < 1$) lead to the formation of an insoluble MoO_3 oxide [76], which acts as an n-type semiconductor [77, 78]; although, the n-type semiconductor properties can also be attributed to the presence of other compounds, such as Fe_2O_3 [36, 77, 78]. Regarding the role of Mo, Montemor et al. [38], based on Auger analysis, reported that this element has no significant effect on the oxide thickness; however, the presence of Mo as an alloying element in stainless steel leads to a higher amount of Cr in the inner oxide layer. These results have also been observed in other works [79, 80] and, therefore, this suggests a chromium-enriched inner layer that behaves as an n-type semiconductor. However, Tsuchiya et al. [81] concluded that the passive film on Cr and Fe-Cr alloys can display both an n-type and a p-type behaviour in acidic media, due to the double layer structure in the film and therefore, the n-type semiconducting behaviour of Alloy 31 can be mainly attributed to the chromium-enriched inner layer.

On the other hand, the Mott-Schottky diagram in **Figure 6d** represents the properties of passive films formed at $1 \text{ V}_{\text{Ag}/\text{AgCl}}$ and different temperatures, in which three regions are distinguished. The negative slopes in region I are attributed to a p-type behaviour, probably due to the presence of Cr_2O_3 , FeO and NiO on the passive films [36], and this behaviour is observed at all temperatures, in contrast to those obtained at 0.3, 0.5 and $0.8 \text{ V}_{\text{Ag}/\text{AgCl}}$. Region II presents positive slopes, which depicts an n-type semiconducting behaviour (**Figures 6a, b and c**). However, the difference in these diagrams is the appearance of a third region, with a peak at around $0.5 \text{ V}_{\text{Ag}/\text{AgCl}}$. This feature has been usually explained in terms of a strong dependence of the Faradaic current on potential in

the transpassive region. In this sense, the behaviour of capacitance at high potentials near the transpassive region has been attributed to the development of an inversion layer as a result of an increasing concentration in the valence band; under these conditions, the passive film becomes conductive or thinner due to transpassivation [25, 82-84]. This is consistent with the results obtained from the EIS measurements and agrees well with the polarisation curve results, in which the transpassive region at all temperatures was found to be close to 1 V_{Ag/AgCl}.

According to Eq. (7) donor densities, N_D , can be determined from the slope of the experimental C^2 versus E plots. Because the slope is inversely proportional to the donor density, the decrease in the slope when temperature increases indicates that the concentration of donor species in the passive film increases with temperature [4], which implies that high donor densities lead to high passive current density values in the passive region, according to the polarisation curves. The values of donor densities corresponding to Alloy 31 are summarised in **Table 3** and they are all of the order of 10^{20} cm⁻³, which agree well with those reported for austenitic stainless steels [4, 28, 34, 39]. Higher donor density values at elevated temperatures means that the passive film on Alloy 31 has higher electron density and lower impedance, as observed in the EIS measurements.

For all the four temperatures studied, the donor density decreases with increasing formation potential, except above 0.8 V. These results are consistent with other reports [32, 33, 85, 86]. At potentials higher than 0.8 V, donor densities show a small increase due to the loss of passivity in Alloy 31. This tendency of the donor density to decrease with increasing potential has been reported by Sikora and Macdonald [29], who

reported that the relationship between N_D and the formation potential was correctly predicted on the basis of the Point Defect Model (PDM), assuming that the oxygen vacancies are the electron donors. Other studies have also developed this relationship by using the PDM [85, 86].

Finally, acceptor density, N_A , has been determined from the negative slopes in region I of **Figure 6d**, according to Eq. (6). Acceptor density values are summarised in **Table 3** and they are observed to increase with temperature. Based on the values of **Table 3**, it can be concluded that the passive film on Alloy 31 is disordered and becomes more visible at higher temperatures, as expected. The donors or acceptors in semiconducting passive layers are defects, including cation vacancies, anion vacancies, and cation interstitials. These vacancies act as dopants, i.e. oxygen vacancies and cation interstitials imparting n-type properties and cation vacancies yielding p-type character. The presence of such dopants prevents migration of cations from substrate metal and alloys and penetration of harmful anions, such as Cl^- and SO_4^{2-} , from the electrolyte, thereby improving corrosion resistance [9, 27, 87].

These results are consistent with both polarisation curves and EIS measurements, revealing that an increase in temperature results in a more disordered passive film. However, Alloy 31 in the phosphoric acidic solution still provides high corrosion resistance at elevated temperatures.

4. CONCLUSIONS

The electrochemical behaviour of a highly-alloyed austenitic stainless steel (Alloy 31) was investigated in a contaminated phosphoric acid solution at different temperatures. Polarisation curves revealed that Alloy 31 exhibits a wide domain of passivity, ranging between 0.3 and 1 V_{Ag/AgCl}. The high current densities registered in the passive region as temperature increases indicated the thickening of the passive film on Alloy 31.

EIS measurements showed that the protection provided by the passive film was predominantly due to the inner oxide film, while R_f values demonstrated that the outer film can be considered as thin and porous. The influence of temperature and formation potential was observed to affect more markedly the parameters associated with the inner oxide film. An increase in temperature indicates higher electrical conductivity, whereas an increase in capacitance may indicate a thinner film. However, the high values of capacitances and resistances suggested that the film on Alloy 31 still provides significant protection.

The Mott-Schottky plots obtained when Alloy 31 was pre-passivated at 0.3, 0.5 and 0.8 V_{Ag/AgCl}, only showed an n-type-electronic behaviour, while those at 1 V_{Ag/AgCl} showed both a p-type and an n-type behaviour. This fact confirmed the growth of an inversion layer as a consequence of the proximity to the transpassivation region. Calculated acceptor/donor densities of Alloy 31 in the contaminated phosphoric acid, revealed an increase of the acceptor/donor density with temperature and they are all of the order of 10^{20} cm^{-3} .

5. ACKNOWLEDGEMENTS

The authors wish to express their gratitude to the MAEC of Spain (PCI Mediterráneo C/8196/07, C/018046/08, D/023608/09 and D/030177/10, to Programa de Apoyo a la Investigación y Desarrollo de la UPV (PAID-06-09), to the Generalitat Valenciana (GV/2011/093) for the financial support and to Dra. Asunción Jaime for her translation assistance.

6. REFERENCES

- [1] I. Olefjord, B. O. Elfstrom, *Corrosion* 38 (1982) 46.
- [2] C. O. A. Olsson, D. Landolt, *Electrochim. Acta* 48 (2003) 1093.
- [3] L. Freire, M. J. Carmezim, M. G. S. Ferreira, M. F. Montemor, *Electrochim. Acta* 55 (2010) 6174.
- [4] M. J. Carmezim, A. M. Simoes, M. F. Montemor, M. D. Cunha Belo, *Corros. Sci.* 47 (2005) 581.
- [5] N. E. Hakiki, M. F. Montemor, M. G. S. Ferreira, M. da Cunha Belo, *Corros. Sci.* 42 (2000) 687.
- [6] F. Gaben, B. Vuillemin, R. Oltra, *J. Electrochem. Soc.* 151 (2004) B595.
- [7] H. Ha, H. Jang, H. Kwon, S. Kim, *Corros. Sci.* 51 (2009) 48.
- [8] N. E. Hakiki, M. D. Belo, A. M. P. Simoes, M. G. S. Ferreira, *J. Electrochem. Soc.* 145 (1998) 3821.
- [9] Y. X. Qiao, Y. G. Zheng, W. Ke, P. C. Okafor, *Corros. Sci.* 51 (2009) 979.
- [10] T. L. Sudesh, S. Wijesinghe, D. J. Blackwood, *Corros. Sci.* 50 (2008) 23.
- [11] E. Almeida, D. Pereira, M. O. Figueiredo, V. M. M. Lobo, M. Morcillo, *Corros. Sci.* 39 (1997) 1561.
- [12] S. R. Moraes, D. Huerta-Vilca, A. J. Motheo, *Prog. Org. Coat.* 48 (2003) 28.

- [13] M. Reffass, R. Sabot, M. Jeannin, C. Berziou, P. Refait, *Electrochim. Acta* 54 (2009) 4389.
- [14] A. Bellaouchou, A. Guenbour, A. Benbachir, *Corrosion* 49 (1993) 656.
- [15] A. Bellaouchou, A. Guenbour, A. Benbachir, *Bull. Electrochem.* 16 (2000) 166.
- [16] S. El Hajjaji, L. Aries, J. Audouard, F. Dabosi, *Corros. Sci.* 37 (1995) 927.
- [17] A. Guenbour, M. A. Hajji, E. M. Jallouli, A. B. Bachir, *Appl. Surf. Sci.* 253 (2006) 2362.
- [18] M. Lakatos-Varsányi, F. Falkenberg, I. Olefjord, *Electrochim. Acta* 43 (1998) 187.
- [19] S. Magaino, M. Matlosz, D. Landolt, *J. Electrochem. Soc.* 140 (1993) 1365.
- [20] M. Matlosz, S. Magaino, D. Landolt, *J. Electrochem. Soc.* 141 (1994) 410.
- [21] M. Michael, *Electrochim. Acta* 40 (1995) 393.
- [22] I. Betova, M. Bojinov, T. Tzvetkoff, *Appl. Surf. Sci.* 220 (2003) 273.
- [23] K. Prabakaran, S. Rajeswari, *J. Appl. Electrochem.* 39 (2009) 887.
- [24] R. Babic, M. Metikos-Hukovic, *J. Electroanal. Chem.* 358 (1993) 143.
- [25] A. Di Paola, *Electrochim. Acta* 34 (1989) 203.
- [26] A. Di Paola, D. Shukla, U. Stimming, *Electrochim. Acta* 36 (1991) 345.
- [27] N. B. Hakiki, S. Boudin, B. Rondot, M. Cunha Belo, *Corros. Sci.* 37 (1995) 1809.
- [28] M. Metikos-Hukovic, R. Babic, Z. Grubac, Z. Petrovic, N. Lajci, *Corros. Sci.* 53 (2011) 2176.
- [29] E. Sikora, D. D. Macdonald, *Solid State Ionics* 94 (1997) 141.
- [30] J. Sikora, E. Sikora, D. D. Macdonald, *Electrochim. Acta* 45 (2000) 1875.
- [31] D. D. Macdonald, *J. Electrochem. Soc.* 153 (2006) B213.

- [32] A. Fattah-alhosseini, M. A. Golozar, A. Saatchi, K. Raeissi, *Corros. Sci.* 52 (2010) 205.
- [33] A. Fattah-alhosseini, F. Soltani, F. Shirsalimi, B. Ezadi, N. Attarzadeh, *Corros. Sci.* 53 (2011) 3186.
- [34] M. G. S. Ferreira, N. E. Hakiki, G. Goodlet, S. Faty, A. M. P. Simoes, M. Cunha Belo, *Electrochim. Acta* 46 (2001) 3767.
- [35] N. Li, Y. Li, S. Wang, F. Wang, *Electrochim. Acta* 52 (2006) 760.
- [36] X. Cheng, X. Li, C. Du, *Chin. Sci. Bull.* 54 (2009) 2239.
- [37] L. V. Taveira, M. F. Montemor, M. Cunha Belo, M. G. Ferreira, L. F. P. Dick, *Corros. Sci.* 52 (2010) 2813.
- [38] M. F. Montemor, A. M. Simoes, M. G. S. Ferreira, M. D. C. Belo, *Corros. Sci.* 41 (1999) 17.
- [39] H. Jang, H. Kwon, *J. Electroanal. Chem.* 590 (2006) 120.
- [40] H. Iken, R. Basseguy, A. Guenbour, A. B. Bachir, *Electrochim. Acta* 52 (2007) 2580.
- [41] Pierre Becker, *Phosphates and phosphoric acid. Raw materials, technology, and economics of the wet process*, M. Dekker New York, 1989.
- [42] ASTM G-5, *Test Method for Making Potentiostatic and Potentiodynamic Anodic Polarization Measurements*, ASTM 2004.
- [43] Y. X. Qiao, Y. G. Zheng, P. C. Okafor, W. Ke, *Electrochim. Acta* 54 (2009) 2298.
- [44] E. Blasco-Tamarit, A. Igual-Muñoz, J. García Antón, D. García-García, *Corros. Sci.* 50 (2008) 1848.
- [45] M. Ibáñez-Ferrándiz, M. Blasco-Tamarit, D. M. García-García, J. García-Antón, A. Guenbour, S. Bakour, A. Benckokroun, *ECS Trans.* 25 (2010) 49.

- [46] C. Escrivà-Cerdán, E. Blasco-Tamarit, D. M. García-García, J. García-Antón, A. Guenbour, *Corros. Sci.* 56 (2012) 114.
- [47] L. F. Garfias-Mesias, J. M. Sykes, *Corros. Sci.* 41 (1999) 959.
- [48] A. Igual Muñoz, J. García Antón, S. López Nuévalos, J. L. Guiñón, V. Pérez Herranz, *Corros. Sci.* 46 (2004) 2955.
- [49] N. J. Laycock, *Corrosion* 55 (1999) 590.
- [50] A. Pardo, E. Otero, M. C. Merino, M. D. Lopez, M. V. Utrilla, F. Moreno, *Corrosion* 56 (2000) 411.
- [51] D. H. Hur, Y. S. Park, *Corrosion* 62 (2006) 745.
- [52] A. Igual-Muñoz, J. García-Antón, J. L. Guiñón, V. Pérez-Herranz, *Corros. Sci.* 48 (2006) 3349.
- [53] M. V. Cardoso, S. T. Amaral, E. M. A. Martini, *Corros. Sci.* 50 (2008) 2429.
- [54] B. Evgenij and R. M. J, *Impedance Spectroscopy: Theory, Experiment and Applications*, West Sussex, UK, 2005.
- [55] M. Urquidi-Macdonald, S. Real, D. D. Macdonald, *J. Electrochem. Soc.* 133 (1986) 2018.
- [56] M. Urquidi-Macdonald, S. Real, D. D. Macdonald, *Electrochim. Acta* 35 (1990) 1559.
- [57] S. L. d' Assis, S. Wolyneć, I. Costa, *Electrochim. Acta* 51 (2006) 1815.
- [58] J. Pan, C. Leygraf, R. F. A. Jargelius-Pettersson, J. Linden, *Oxid. Met.* 50 (1998) 431.
- [59] K. Jüttner, *Electrochim. Acta* 35 (1990) 1501.
- [60] S. Yagi, A. Sengoku, K. Kubota, E. Matsubara, *Corros. Sci.* 57 (2012) 74.
- [61] H. Huan, Z. Tao, Z. Chengzhi, H. Kai, M. Gouzhe, S. Yawei, W. Fuhui, *J. Appl. Electrochem.* 39 (2009) 737.

- [62] R. Fuchs-Godec, M. G. Pavlovic, *Corros. Sci.* 58 (2012) 192.
- [63] N. P. Cosman, K. Fatih, S. G. Roscoe, *J. Electroanal. Chem.* 574 (2005) 261.
- [64] G. J. Brug, A. L. G. Vandeneeden, M. Sluytersrehabach, J. H. Sluyters, *J. Electroanal. Chem.* 176 (1984) 275.
- [65] C. Valero Vidal, A. Igual Muñoz, *Electrochim. Acta* 55 (2010) 8445.
- [66] G. Blanco, A. Bautista, H. Takenouti, *Cem. Concr. Compos.* 28 (2006) 212.
- [67] M. Bojinov, G. Fabricius, P. Kinnunen, T. Laitinen, K. Mäkelä, T. Saario, G. Sundholm, *J. Electroanal. Chem.* 504 (2001) 29.
- [68] O. Han-Jun, S. Choong-Soo, *Bull. Korean Chem. Soc.* 21 (2000) 193.
- [69] R. M. Fernández-Domene, E. Blasco-Tamarit, D. M. García-García, J. García-Antón, *Corros. Sci.* 55 (2012) 40.
- [70] L. Freire, M. J. Carmezim, M. G. S. Ferreira, M. F. Montemor, *Electrochim. Acta* 56 (2011) 5280.
- [71] D. D. Macdonald, A. Sun, N. Priyantha, P. Jayaweera, *J. Electroanal. Chem.* 572 (2004) 421.
- [72] J. Pan, D. Thierry, C. Leygraf, *Electrochim. Acta* 41 (1996) 1143.
- [73] R. Degryse, W. P. Gomes, F. Cardon, J. Vennik, *J. Electrochem. Soc.* 122 (1975) 711.
- [74] G. Lothongkum, S. Chaikittisilp, A. W. Lothongkum, *Appl. Surf. Sci.* 218 (2003) 203.
- [75] D. D. Macdonald, *J. Electrochem. Soc.* 139 (1992) 3434.
- [76] A. Pardo, M. C. Merino, A. E. Coy, F. Viejo, R. Arrabal, E. Matykina, *Corros. Sci.* 50 (2008) 780.
- [77] C. Sunseri, S. Piazza, F. Di Quarto, *J. Electrochem. Soc.* 137 (1990) 2411.
- [78] M. H. Dean, U. Stimming, *Corros. Sci.* 29 (1989) 199.

- [79] H. Habazaki, A. Kawashima, K. Asami, K. Hashimoto, *Corros. Sci.* 33 (1992) 225.
- [80] M. W. Tan, E. Akiyama, A. Kawashima, K. Asami, K. Hashimoto, *Corros. Sci.* 37 (1995) 1289.
- [81] H. Tsuchiya, S. Fujimoto, O. Chihara, T. Shibata, *Electrochim. Acta* 47 (2002) 4357.
- [82] U. Stimming, J. W. Schultze, *Berichte der Bunsen-Gesellschaft, Phys. Chem. Chem. Phys.* 80 (1976) 1297.
- [83] S. U. M. Khan, W. Schmickler, *J. Electroanal. Chem. Interfacial Electrochem.* 108 (1980) 329.
- [84] D. M. Tench, E. Yeager, *J. Electrochem. Soc.* 120 (1973) 164.
- [85] S. J. Ahn, H. S. Kwon, *Electrochim. Acta* 49 (2004) 3347.
- [86] E. Sikora, J. Sikora, D. D. Macdonald, *Electrochim. Acta* 41 (1996) 783.
- [87] E. Cho, H. Kwon, D. D. Macdonald, *Electrochim. Acta* 47 (2002) 1661.

Table 1. Chemical composition of the UNS N08031 (Alloy 31) (wt.%).

	%Cr	%Fe	%Ni	%Mo	%Mn	%Cu	%N	%Si	%C	%S	%P
Alloy 31	26.75	31.43	31.85	6.6	1.5	1.21	0.193	0.1	0.005	0.002	0.017

Table 2. Electrical parameters obtained by fitting the experimental results of EIS for Alloy 31 in the contaminated 40 wt.% H₃PO₄ solution at different temperatures after passive film formation at different potentials.

E vs (Ag/AgCl) / V	t / °C	$10^6 Q_1 / \Omega^{-1} \text{cm}^{-2} \text{s}^n$	α_1	$R_1 / \text{K}\Omega \text{cm}^2$	$C_{1dl} / \mu\text{F}\cdot\text{cm}^{-2}$	$10^6 Q_2 / \Omega^{-1} \text{cm}^{-2} \text{s}^n$	α_2	$R_2 / \text{K}\Omega \text{cm}^2$	$C_2 / \mu\text{F}\cdot\text{cm}^{-2}$
0.3	20	43.33	0.920	1.23	34.07	51.31	0.734	61.53	77.82
	40	42.61	0.915	0.76	29.66	65.85	0.698	25.64	82.64
	60	40.08	0.934	0.58	28.74	80.75	0.596	10.86	73.87
	80	53.45	0.902	0.67	40.39	112.30	0.810	4.06	93.39
0.5	20	33.61	0.926	0.92	25.28	48.00	0.682	64.85	81.51
	40	25.31	0.948	0.63	19.93	54.61	0.654	62.34	104.32
	60	30.69	0.926	0.50	21.95	69.07	0.745	46.87	103.31
	80	35.66	0.935	0.30	25.99	79.84	0.681	20.33	100.20
0.8	20	32.25	0.906	0.86	22.23	52.00	0.781	95.72	81.77
	40	26.38	0.930	0.52	19.10	52.13	0.670	81.39	107.23
	60	23.355	0.934	0.41	16.80	52.60	0.652	67.16	102.74
	80	38.206	0.916	0.28	25.20	85.25	0.690	21.51	111.56
1	20	86.99	0.8605	1.14	59.80	93.29	0.7122	61.81	189.38
	40	105.94	0.8518	1.26	74.62	125.73	0.7381	39.57	222.17
	60	123.56	0.8417	0.79	79.73	168.40	0.7462	16.99	240.77
	80	110.80	0.9574	0.58	98.06	235.51	0.6210	5.06	262.18

Table 3. Donor and acceptor density (N_D / N_A) of the oxide films formed on Alloy 31 at different formation potential and temperatures between 20 and 80 °C.

Parameters			
E vs (Ag/AgCl) / V	t / °C	$N_D / 10^{20} \text{ cm}^{-3}$	$N_A / 10^{20} \text{ cm}^{-3}$
0,3	20	4.22	
	40	4.50	
	60	4.58	
	80	5.96	
0,5	20	2.77	
	40	3.00	
	60	3.02	
	80	3.07	
0,8	20	2.65	
	40	2.72	
	60	2.94	
	80	3.37	
1	20	8.58	22.76
	40	10.66	32.72
	60	11.34	45.98
	80	12.14	79.62

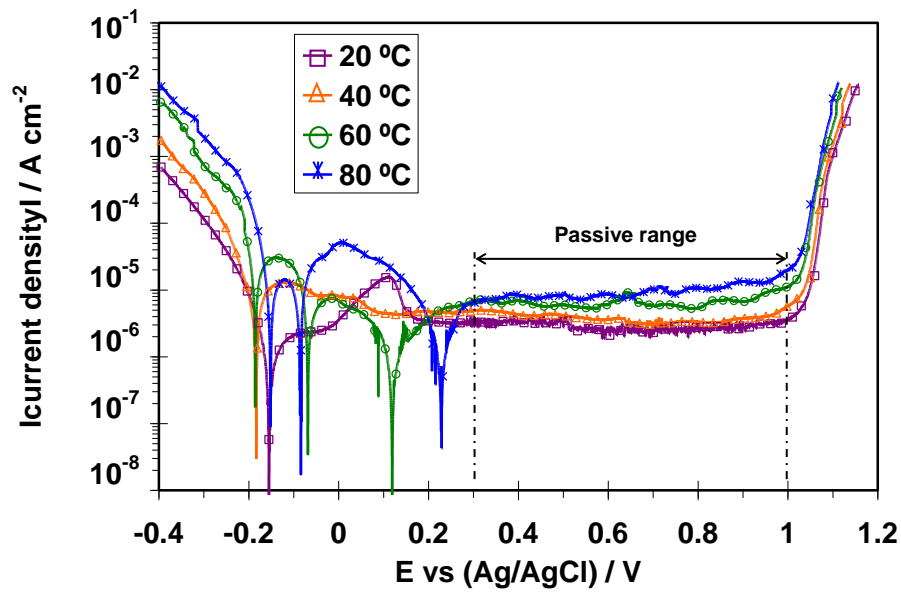


Figure 1. Potentiodynamic polarisation curves of Alloy 31 in 40 wt.% H₃PO₄ polluted with 2 wt.% H₂SO₄ and 0.06 wt.% KCl at different temperatures.

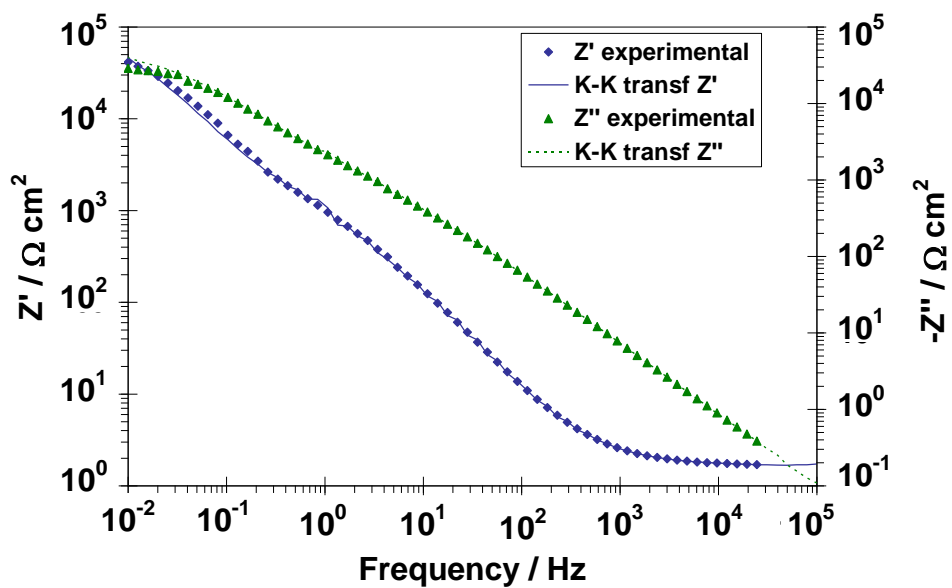
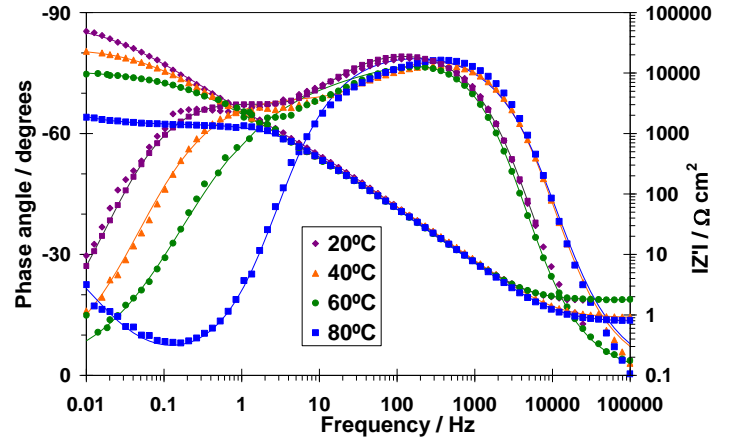
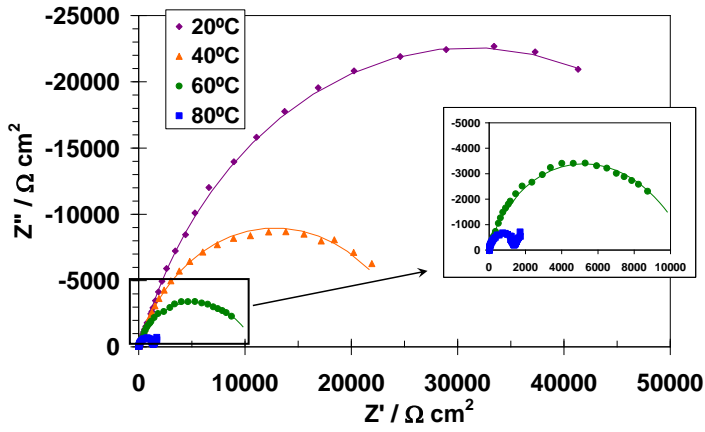
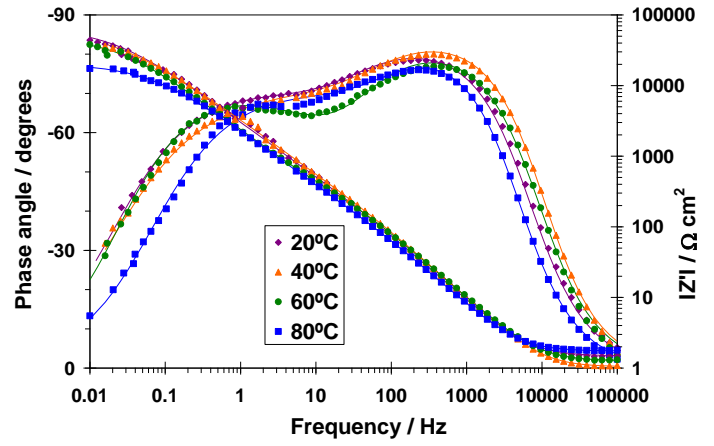
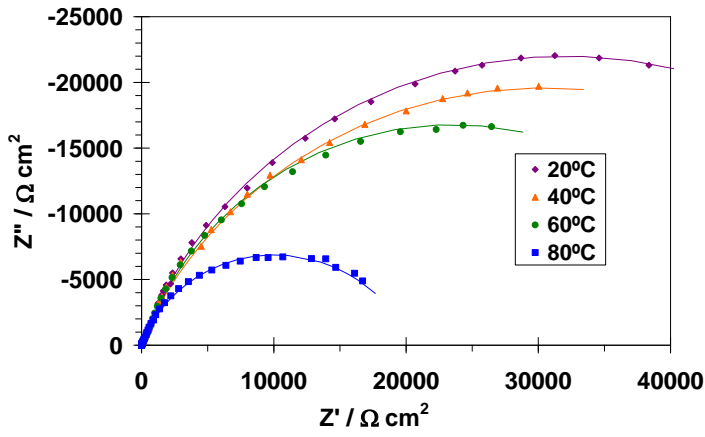


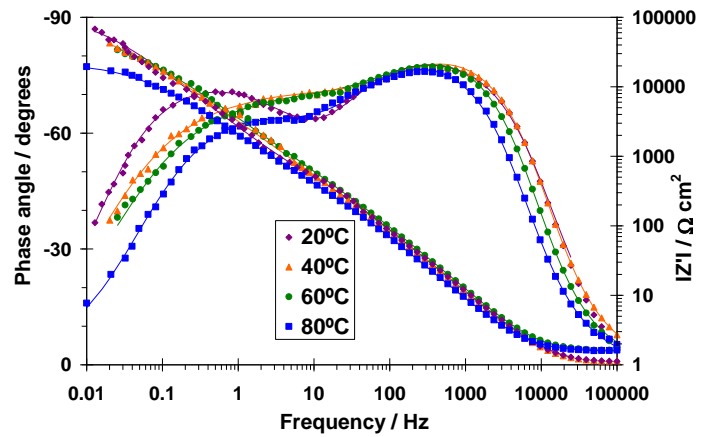
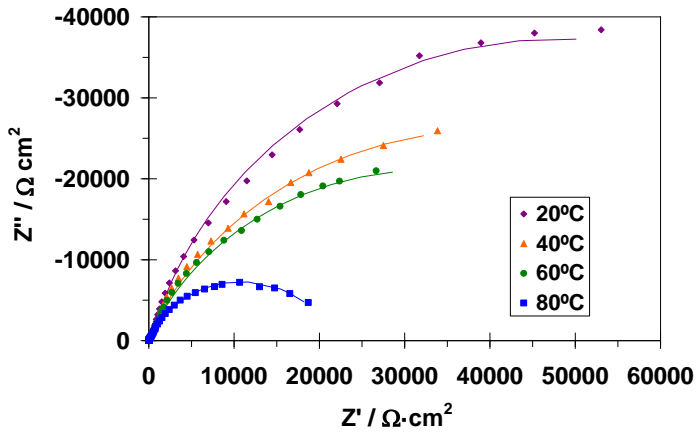
Figure 2. Kramers-Kronig transformation of the impedance diagram obtained after 1h of stabilisation at $0.3 V_{Ag/AgCl}$ and $20\text{ }^{\circ}\text{C}$ in 40 wt.% H_3PO_4 polluted with 2 wt.% H_2SO_4 and 0.06 wt.% KCl .



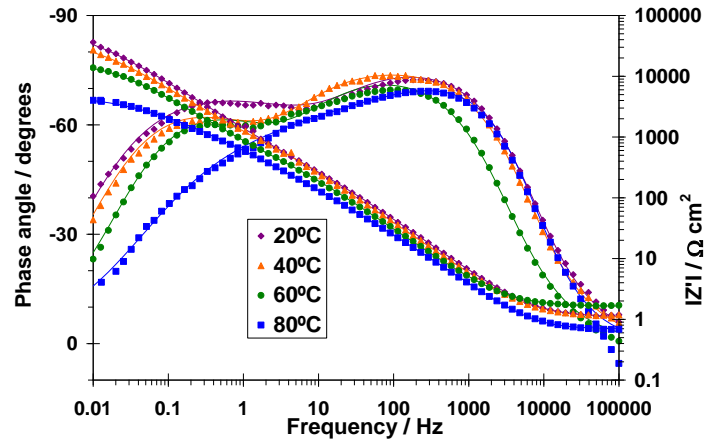
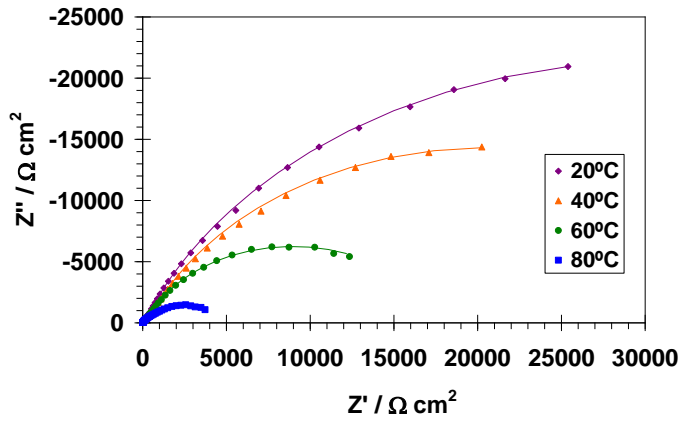
(a)



(b)



(c)



(d)

Figure 3. Nyquist diagrams (left) and Bode plots (right) of Alloy 31 after 1h of immersion at (a) 0.3, (b) 0.5, (c) 0.8 and (d) 1 $V_{Ag/AgCl}$ in the polluted H_3PO_4 solution with 2 wt.% H_2SO_4 and 0.06 wt.% KCl at different temperatures.

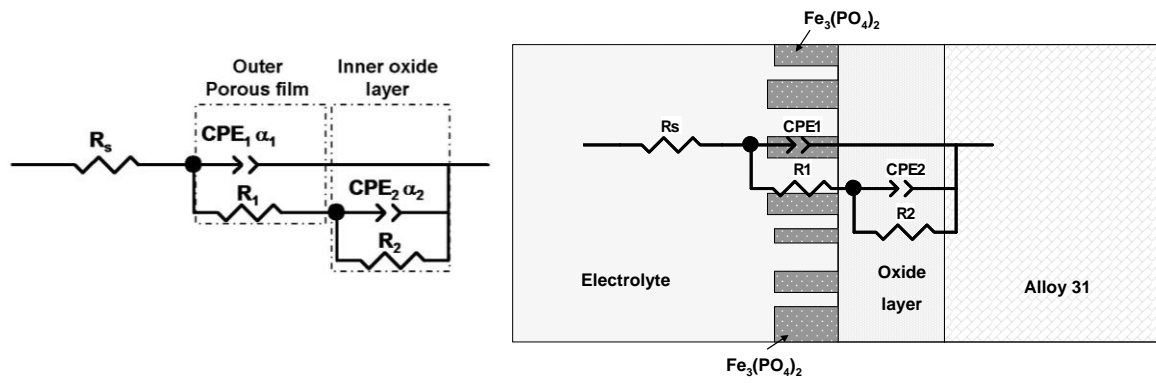


Figure 4. Equivalent electric circuit tested to model the experimental EIS data with two hierarchically distributed time constants. Schematic representation of Alloy 31 oxide film and porous layer of phosphates and physical interpretation of the circuit.

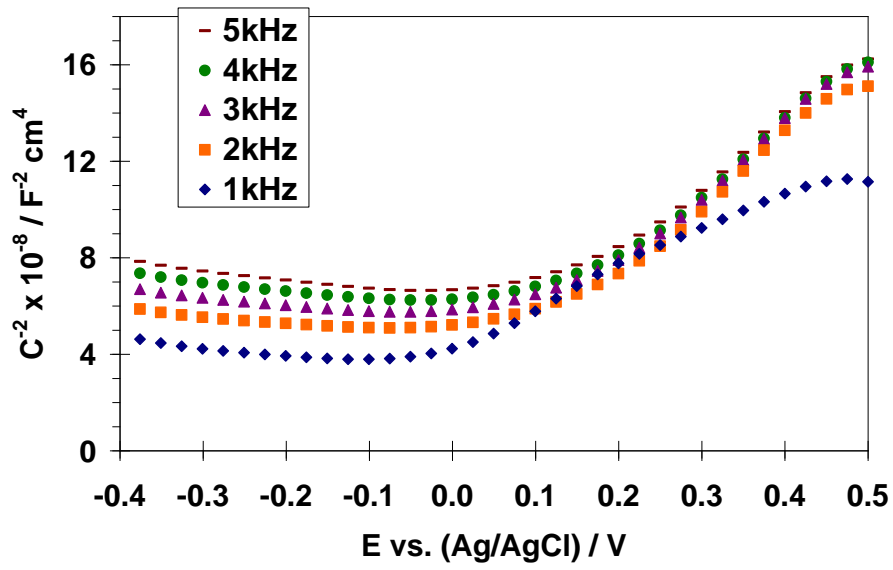


Figure 5. Capacitance vs. potential curves obtained for Alloy 31 in the contaminated H_3PO_4 solution at different frequencies.

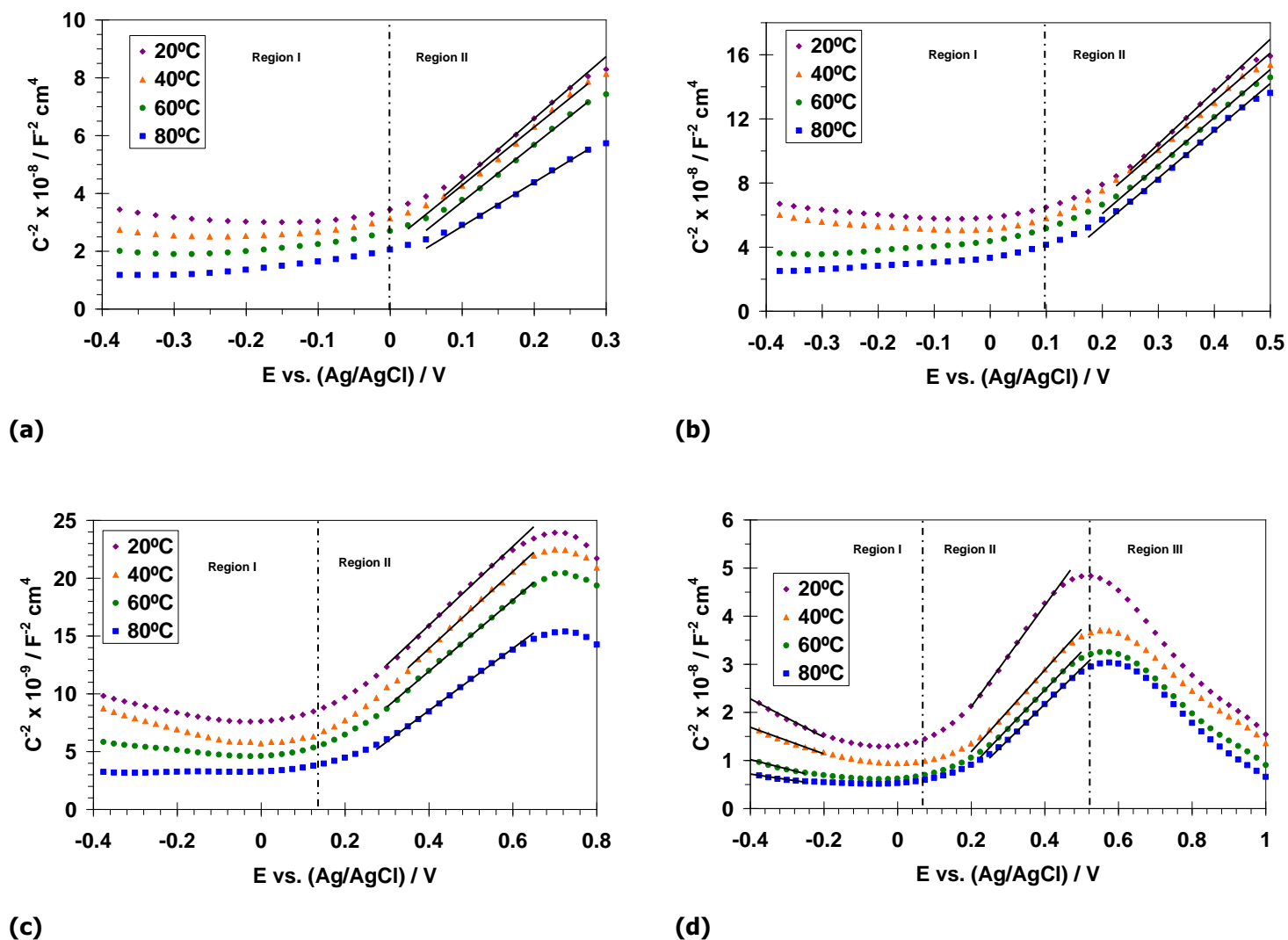


Figure 6. Mott-Schottky plots of passive films formed on Alloy 31 at different temperatures and after the anodisation process for 1 h at (a) 0.3, (b) 0.5, (c) 0.8 and (d) 1 V vs. Ag/AgCl, in the 40 wt.% H_3PO_4 polluted solution with 2 wt.% H_2SO_4 and 0.06 wt.% KCl.